



Erythrocyte-biomimetic nanosystems to improve antitumor effects of paclitaxel on epithelial cancers

Mingming Song^{a,b,1}, Shuqi Dong^{a,1}, Xiaofei An^c, Wenxiang Zhang^a, Ning Shen^d, Yanbo Li^e, Caixia Guo^f, Chang Liu^a, Xiao Li^{b,*}, Siyu Chen^{a,*}

^a State Key Laboratory of Natural Medicines and School of Life Science and Technology, China Pharmaceutical University, Nanjing, China

^b Department of Pathology, First Affiliated Hospital with Nanjing Medical University, Nanjing, Jiangsu, China

^c Department of Endocrinology, Affiliated Hospital of Nanjing University of Chinese Medicine, Nanjing, China

^d China Exposomics Institute, Shanghai, China

^e Department of Toxicology and Sanitary Chemistry, School of Public Health, Capital Medical University, Beijing, China

^f Beijing Key Laboratory of Environmental Toxicology, Capital Medical University, Beijing, China

ARTICLE INFO

Keywords:

Epithelial malignancy
Erythrocyte membrane
Biomimetic nanoparticles
Paclitaxel
Systemic toxicity

ABSTRACT

Chemotherapy is a difficult treatment for cancer patients because of the low effective accumulation of chemodrugs and their detrimental side effects. Nanoparticles have shown promise as a solution to these problems. However, the known differences in the porosity and vascularization of tumor vessels, and other factors, including the potential formation of a “protein crown,” the short half-life time in circulation, and the low drug distribution, often limit their application. To address these problems, biomimetic nanoparticles coated with cell membranes have been developed and shown to have advantages such as prolonged circulation, high biocompatibility, and enhanced targeting abilities in drugs and nanoparticles, thus exhibiting good application prospects in cancer therapy for liver, lung, and melanoma cancers. Accordingly, we designed a PH-sensitive biomimetic nanodrug delivery system with a delicate “core-shell” structure based on red blood cell membranes. Briefly, core nanoparticles were synthesized by the self-assembly of natural amphoteric polymers, including hydrophilic carboxymethylcellulose sodium and hydrophobic stearic acid. For the shell structure, red blood cell membranes were modified using folic acid by a lipid tether (1,2-distearoyl-sn-glycero-3-phosphoethanolamine) to increase tumor-targeting ability, whereas polyethylene glycol was inserted to decrease lipid tether modification-induced potential sequestration by either the mononuclear phagocyte system or the reticuloendothelial system. Via a series of formulation optimizations, paclitaxel was packaged into the red blood membrane-based core-shell nanoparticles with an average size of 226.9 ± 2.75 nm and a negative Zeta potential of -14.5 ± 0.3 mV. More importantly, the examinations focusing on CD47, a representative red blood cell membrane protein, revealed not only the successful establishment of the membrane shell but also the right-side-out membrane orientation on our core-shell nanoparticles. Our nanodrug delivery system showed good biocompatibility and sensitivity to acidic tumor microenvironments while effectively prolonging the circulation time of paclitaxel and further enhancing its antitumor effects on epithelial malignancies, including liver, lung, and melanoma cancers. In particular, our nanodrug delivery system significantly alleviated paclitaxel-induced renal toxicity. Taken together, our findings highlight that the red blood membrane-based core-shell nanoparticle is a promising biomimetic nanodrug delivery system for functionally delivering chemotherapeutic drugs, and it has promise in clinical applications.

1. Introduction

Epithelial malignancies account for more than 85% of human malignancies and threaten public health [1]. For decades, scientists have

struggled to remedy this and have developed multiple countermeasures, including surgery, chemotherapy, radiation therapy, phototherapy, and gene therapy [2–4]. Although these strategies have exhibited some ability to inhibit tumor growth, the prognosis of epithelial malignancy is

* Corresponding authors.

E-mail addresses: lxiao@njmu.edu.cn (X. Li), siyuchen@cpu.edu.cn (S. Chen).

¹ These authors contributed equally to this work.

still poor and accompanied by a high mortality rate in tumor patients [5].

Chemotherapy is a difficult treatment for cancer patients because of unexpected and detrimental side effects [6,7]. Among them, paclitaxel (PTX) is a first-line chemotherapeutic agent extracted from the *Pacific yew tree* [8]. It targets tubulin to reduce the dynamics of intracellular microtubule networks, thereby inhibiting tumor cell proliferation and promoting cell apoptosis and necrosis. Further, it has been successfully applied to the clinical treatment of liver cancer, lung cancer, and melanoma [9–11]. However, the buckets effect of PTX also exists because of its short half-life, strong hydrophobicity, and high systemic toxicity, especially in the kidney [12–14]. Therefore, overcoming the shortcomings of PTX application would improve its clinical efficacy in the treatment of malignant epithelial tumors.

With the development of modern nanoscience and biotechnology, artificial nanomaterials and nanoplateforms have been used in cancer treatment [15,16]. These nanoparticles (NPs) are used for a functional and safe nanodrug delivery system (NDDS) to improve multiple aspects of chemotherapeutic drugs, including water solubility, absorption, metabolism, distribution, excretion, and toxicity [17]. Moreover, the tumor-targeting ability of NDDS plays a critical role in minimizing the side effects and improving the therapeutic efficacy of chemotherapeutic drugs [18]. To localize NPs to tumor tissues, many strategies have been applied, including but not limited to, the following: 1. optimizing the size of NPs, which allows passive accumulation of drugs in tumor tissues via leaky vasculature based on the enhanced permeability and retention effect (EPR) [19], 2. incorporating targeting moieties for binding NPs to cancer cells (active transpiration) [20]. For instance, modification of FA is considered a functional strategy for improving the targeting efficacy of NDDS while decreasing the undesired biodistribution in peripheral organs [21]. Because of the high expression of folate receptors on the membrane of cancer cells, folic acid (FA) functions as an energy source to maintain their uncontrollable proliferation [22]. Collectively, NDDS not only serves as a protective carrier for therapeutic drugs but also provides additional benefits, including prolonged circulating times/sustained drug release, increased tumor-targeting abilities, and reduced chemotherapeutic drug-induced organ toxicity [23].

In past decades, organic materials, such as poly(lactic-co-glycolic acid) (PLGA) [24] and poly(caprolactone) (PCL) [25], have functioned as basal sources for establishing NDDS. However, owing to the low drug loading capacity (typically <10%) [26], large quantities of these formulations are required to encapsulate drug payloads [27]. Meanwhile, high doses of these materials increase the risk of potential toxicities and trigger an active immune response [28], which may aggravate cancer progression. In contrast, natural materials exhibit good biocompatibility and low toxicity. For example, polysaccharides are natural molecules with flexible modified functional groups that are prone to coupling with NPs and other small molecules; hence, they possess great potential for drug delivery, cancer treatment, and diagnosis [29,30]. Among polysaccharides, carboxymethylcellulose sodium (CMC) is chemically modified from natural polysaccharide cellulose and has been widely used in the oral delivery of hydrophobic drugs [31,32]. Notably, CMC is highly sensitive to acidic tumor environments, increasing its potential for the delivery of chemotherapeutic drugs into tumor tissues [33]. Additionally, stearic acid (SA) is an endogenous metabolite involved in lipid metabolism. Given its hydrophobic properties, it can serve as a facilitator to increase drug solubility and enhance the loading efficacy of NPs. Notably, due to biological barriers, only 0.7% (median) of administered NPs are delivered to solid tumors [34]. However, unsolved problems, including insufficient resident time, the unavoidable synthesis of a “protein crown,” the nonspecific uptake by liver and kidney, clearance by host immune system, and poor penetration into tumor tissues, limit the clinical applications of organic material-based NDDS [35]. Therefore, it is important to establish an advanced NDDS to cross physical/biological barriers and increase the antitumor properties of chemo-drugs.

To address these problems, erythrocyte membrane-cloaked NPs were developed in 2011 [36], which paved the way for cell membrane-cloaked NPs [37–39]. Such a new type of biomimetic NDDS combines the unique properties of natural cellular entities, such as a long circulation time. Accordingly, it could dupe the host immune system and avoid the synthesis of, protein crown, thus improving the biocompatibility and prolonging the retention time [40,41]. Among the various types of cell membranes, red blood cell membranes (RBCMs) are the most abundant and biocompatible and are known to penetrate biological barriers. In addition, unique membrane proteins, such as CD47, could help maintain RBC survival in circulation. Many studies have documented the utility of RBCMs in coating drug-loaded polymeric NPs [42]. Although self-derived components and antigen structures exist in/on the RBCM, there is still a lack of related targeting ligands and active transpiration ability in solid tumors. Chemically modifying target ligands, such as FA, is a common method of solving this problem. However, this may lead to the denaturation of functional proteins in RBCM. Accordingly, a nondisruptive functionalization strategy needs to be developed to maintain the integrity of the membrane, which is extremely important for maintaining the cellular function of biomimetic NPs. With the aid of lipid tethers (e.g., 1,2-distearoyl-sn-glycero-3-phosphoethanolamine (DSPE)), targeting ligands can be naturally inserted into RBCMs [43]. Notably, such an insertion could lead to a reduction in NP concealment. Therefore, DSPE-grafted membrane NPs needs to be improved to reduce the possibility of clearance or sequestration by either the mononuclear phagocyte system (MPS) [44] or the reticuloendothelial system (RES) [34].

Herein, we construct a new NDDS with a delicate “core-shell” structure by camouflaging polymer (SA and CMC as basal materials)-assembled NPs with DSPE- polyethylene glycol (PEG)- FA-modified RBCM (FRCS NPs). We found that FRCS NPs exhibited good biocompatibility and were sensitive to acidic tumor microenvironments. Functionally, FRCS NPs effectively improved the therapeutic effects of PTX on epithelial malignancies, including liver cancer, lung cancer, and melanoma. Further, FRCS NPs significantly alleviated PTX-induced toxicity in various organs, especially in the kidneys. Therefore, FRCS NPs offer a safe and efficient carrier for toxic chemotherapeutic drugs for the treatment of epithelial malignancies.

2. Materials and methods

2.1. Materials

Carboxymethylcellulose sodium, folic acid, and stearic acid were purchased from Sangon Biotech Co. Ltd. (Shanghai, China). Filipin, N, N-dicyclohexylcarbodiimide (DCC), 4-(dimethylamino) pyridine (DMAP), (N1-(ethylimino-methylene)-N3, N3-dimethylpropane-1,3-diamine (EDC), N-hydroxysuccinimide (NHS), and dimethyl sulfoxide (DMSO) were obtained from Sigma-Aldrich (St. Louis, MO, USA). DSPE-PEG-folate, carboxymethyl cellulose sodium, stearic acid, PTX, chlorpromazine hydrochloride, and EIPA were obtained from Shanghai Aladdin Bio-Chem Technology Co., Ltd. (Shanghai, China). All the other chemicals and reagents used in this study were of analytical grade.

2.2. Cell lines and animal models

RAW264.7 macrophages cells, HepG2 cells (human hepatocellular carcinoma), A549 cells (human lung epithelial cells), and A375 cells (human malignant melanoma cells) were obtained from ATCC (Manassas, VA, USA). These cells were cultured in DMEM containing 10% fetal bovine serum (FBS) and penicillin/streptomycin (100 µg/mL) and maintained at 37 °C in 5% CO₂ environment. All animal procedures in this study conformed to the Guide for the Care and Use of Laboratory Animals published by the US National Institutes of Health (NIH publication No. 85–23, revised 1996) and the approved regulations set by the Laboratory Animal Care Committee at the China Pharmaceutical

University (Permit number SYXK-2021-0011). Male C57BL/6 J (8 weeks old) and BALB/C-NU mice (5 weeks old) were purchased from the Model Animal Research Center of Nanjing University (Nanjing, China).

2.3. Preparation of erythrocyte membrane-obtained vesicles

Whole blood from healthy C57BL/6 J mice was centrifuged at 3000 rpm for 5 min to remove plasma. The RBCs were washed three times with ice-cold PBS (pH 7.4) and ruptured by suspension in 0.01 mM PBS for 3 h. After centrifugation (13,000 rpm, 10 min, 4 °C), the precipitates were repeatedly washed with ice-cold PBS and centrifuged until the supernatant became colorless. The RBCMs were sonicated in a capped glass vial for 5 min. The resulting vesicles were subsequently extruded serially through 200 nm polycarbonate porous membranes using Millex®-HV (Merck Millipore Ltd., USA).

2.4. RBCM protein characterization

RBCM proteins were extracted from RBCs in accordance with a previous study and identified by SDS-PAGE and Coomassie blue staining analyses [45].

2.5. Preparation of FRCMs

To construct FRCMs, 1 mL RBCM and 10 µL DSPE-PEG-FA (25 mg/mL) were mixed and stirred at 37 °C for 12 h. The unreacted reagents were then removed by dialysis against ddH₂O. The water was replaced every 6 h, and dialysis was continued for 48 h. Finally, the dialysis samples were subjected to vacuum freeze-drying treatment to obtain the FRCMs. To ensure successful DSPE-PEG-FA insertion, the sample was further analyzed using ¹H NMR spectroscopy.

2.6. Synthesis of CMCS NPs

CMCS was synthesized by grafting carboxymethylcellulose with stearic acid via a carbodiimide crosslinking reaction. Carboxymethylcellulose (50 mg) was dissolved in ddH₂O, and 10 mg of EDC and 5 mg of NHS were added and stirred at 25 °C for 2 h to activate the carboxyl group. Furthermore, 25 mg of stearic acid was dissolved in 5 mL of ethanol at 50 °C and stirred for 0.5 h. Finally, 5 mL of stearic acid was added to the CMC solution, and the reaction was continuously stirred for 24 h at room temperature. The product solution was dialyzed (MW 3500 Da) against deionized water for 3 days. The supernatant was freeze-dried to obtain white-flocculated CMCSs. For the preparation of CMCS NPs, an appropriate amount of CMCS polymer was dissolved in PBS, and the polymer solution was then subjected to contact ultrasound at 75 W for 5 min. Finally, the ultrasound product was filtered with a 0.45 µm microporous membrane and allowed to stand at 37 °C for 12 h to obtain CMCS NPs.

2.7. Preparation and characterization of FRCS NPs

To synthesize PTX FRCS NPs, 10 mg of CMCS and 10 mg of FRCM were mixed and preprocessed by ultrasonic disruption for 5 min to facilitate FRCM coating on the CMCS NPs. Then, 20 mg of PTX was added to the suspension and agitated overnight. The suspension was centrifuged at 12000 rpm for 12 min and washed thrice with PBS to obtain the final PTX FRCS NPs.

2.8. NPs characterization

The hydrodynamic size and zeta potential of the prepared NPs were determined using a Malvern Zetasizer system (ZEN3690; Malvern Instruments Limited, Malvern Worcestershire, UK). The morphology of all the NPs was further confirmed using a transmission electron microscope (HT7700, Hitachi, Tokyo, Japan).

2.9. In vitro release study

Using the dialysis method with a membrane with a molecular weight cutoff of 2000 Da, in vitro drug release kinetics were conducted. Briefly, 1 mL of PTX FRCS NP solution was placed into dialysis tubes and then placed in the release medium (pH 5.5, pH 7.4) at 37 °C, followed by shaking at 150 rpm. At predetermined time points, 100 µL of dissolution medium was collected and supplied with an equal volume of fresh dialysis fluid. The amount of PTX released was measured using UV-Vis spectroscopy. PTX content was quantified by measuring absorbance at 264 nm.

2.10. Sodium dodecyl sulfate-polyacrylamide gel (SDS-PAGE) electrophoresis analysis

SDS-PAGE was used to analyze the proteins. The samples were heated at 100 °C for 7 min, and 45 µg of the sample (source erythrocyte membrane derivation, RBCM NPs, CMCS NPs, and FRCS NPs) was loaded into each well of a 10% SDS-PAGE. The samples were then separated at 120 V for 2 h, and the separation efficacy was examined after the gel was stained with Coomassie brilliant blue.

2.11. Membrane representative protein CD47 expression analysis

CD47 expression was examined by western blotting and FACS analyses. For western blot analysis, SDS-PAGE analysis was performed as described above. Next, the proteins were transferred to a polyvinylidene fluoride (PVDF) membrane, and CD47 protein expression was analyzed using CD47 antibodies (Cat. no. 66304-1-Ig; 1:2000 dilution; Proteintech Group, Inc.). After incubation with the corresponding horse-radish peroxidase-conjugated secondary antibody (Cat. No. SA00001-1; 1:4000 dilution, Proteintech Group, Inc.), protein bands were detected using a Tanon 5200 Multi Fully Automatic Chemiluminescence/Fluorescence Image Analysis System (Tanon, Shanghai, China). For flow cytometric analysis, cell samples were marked using fluorophore-conjugated antimouse antibodies (FITC-tagged anti-N terminal-targeted (extracellular) mouse CD47 antibody, Cat. no. 127503; 1:2000 dilution; BioLegend). The mixture was incubated at room temperature for 2 h and then centrifuged to remove unbound antibody. Flow cytometry was performed using CytoFLEX (Beckman Coulter Inc., CA, USA), and the data were analyzed using FlowJo software version 10.5.3 (Tree Star, Ashland, OR, USA).

2.12. Fluorescence-activated cell sorting (FACS) analysis for the particle internalization of macrophages

RAW264.7 macrophages cells were seeded in 6-well plates at a density of 3×10^5 cells per well. After 24 h, rhodamine B (RhB)/CMCS NPs, RhB/FRCS NPs, and RhB/CD47-blocked FRCS NPs were added to the wells at the same RhB concentration (25 µg/mL). CD47 was blocked using trypsin according to a previously reported method [46]. After 12 h of incubation, the cells were digested, collected, and detected by flow cytometry, and the data were analyzed using FlowJo software version 10.5.3 (FlowJo, Ashland, OR, USA).

2.13. Mechanism of FRCS NPs endocytosis

To investigate the mechanisms involved in FRCS NP uptake by tumor cells (HepG2, A549, and A375 cells), different inhibitors were used to interfere with key uptake pathways. Tumor cells were seeded at a density of 1×10^3 cells/well in a confocal dish containing 4 cm² slides and incubated overnight. To compare the differences in the cellular uptake mechanism, tumor cells were pretreated with culture media containing filipin (1 µg/mL), chlorpromazine (10 µg/mL), EIPA (10 µg/mL), and BafA1 (200 nM) respectively, at 37 °C with 5% CO₂ for 2 h. The culture medium was removed and incubated with full culture medium

containing the same amount of Cy5 FRCS NPs for 24 h. Then, the tumor cells were fixed with 4% paraformaldehyde and the nuclei were stained with DAPI. Finally, the distribution of red fluorescence in tumor cells was observed using CLSM (LSM700, Carl Zeiss, Oberkochen, Germany), and the fluorescence intensity was processed using ZEN imaging software (Carl Zeiss, Oberkochen, Germany).

2.14. *In vivo* biodistribution study

Ectopic tumor models of lung cancer, liver cancer, and melanoma were established as described above. After two weeks, the tumor volume reached 50 mm³. Formulations containing 250 µg/mL Cy5 FRCS NPs were used in all biodistribution studies. For *ex vivo* imaging, mice were administered Cy5 and Cy5 FRCS NPs (Cy5 concentration: 10 mg Cy5 equiv. /kg). After 24 h, the mice were imaged using an IVIS Lumina III *In Vivo* Imaging System (Perkin Elmer, Alameda, USA) with excitation and emission wavelengths of 649 nm and 670 nm, Cy5. Subsequently, the mice were sacrificed, and the main organs, including the heart, liver, spleen, lung, and kidney, were excised and imaged by IVIS using the same settings.

2.15. *In vivo* biocompatibility of FRCS NPs

Healthy C57BL/6 J mice were treated with saline (control) or FRCS nanoparticles (NPs). The mice in the corresponding groups were intravenously administered 100 µL of saline and FRCS NPs. Body weight changes in the mice were recorded during administration. At a pre-determined time, blood was drawn for serum biochemistry and hematologic assays. The major organs were harvested and weighed. After fixation in 4% paraformaldehyde, the tissues were embedded in liquid paraffin and sliced into 5 µm sections for hematoxylin-eosin (H&E) staining.

2.16. *In vitro* cytotoxicity evaluation

The cytotoxicity of FRCS NPs, PTX, and PTX FRCS NPs was evaluated using the CCK-8 assay. Briefly, the tumor cells were plated at a density of 5×10^3 cells in 100 µL per well in 96-well plates and incubated overnight. The culture medium was then replaced with 100 µL of fresh medium containing different concentrations of FRCS NPs, PTX, and PTX FRCS NPs. After another 24-h of incubation, the cells were subjected to the CCK-8 assay according to a previous study.

2.17. *In vivo* antitumor efficacy

When the tumors grew to approximately 50 mm³, tumor-bearing mice were randomly divided into three groups ($n = 5$). PTX and PTX FRCS NPs (PTX 10 mg/kg and equivalent PBS) were injected through the tail vein every 3 day. Tumor volumes ($V = \text{length} \times \text{width} \times \text{width}/2$) and mouse body weights were measured every three days. At the 24th day, the major organs (heart, liver, spleen, lung, and kidneys) and tumor tissues were removed, weighed, rinsed with saline, then fixed with 4% paraformaldehyde solution. Sections were stained with H&E or a one-step TUNEL apoptosis assay kit (Beyotime Biotechnology, Shanghai, China) according to the manufacturer's instructions.

2.18. Serological analysis

Serum samples were collected in centrifuge tubes and centrifuged at 4000 rpm for 10 min at 4 °C. Serum levels of alanine aminotransferase (ALT), aspartate transaminase (AST), blood urea nitrogen (BUN), creatinine (CRE), and inflammatory cytokines, including IL-12, IFN-γ, TNF-α, and IL-6, were determined using commercial kits (Ruixin Biotech, Quanzhou, Fujian, China).

2.19. RT-qPCR analysis

mRNA expression was examined as described in our previous study. Gene expression levels were normalized to 36B4. The qPCR primer sequences for the related genes are listed in Supplementary Table S1.

2.20. Statistical analysis

Data are displayed as mean ± SD. One-way ANOVA with Tukey's post-hoc test was conducted when multiple groups were compared, and Two-tailed paired *t*-test was used to compare two groups. Statistical significance was set at $p < 0.05$. Detailed comparison information were presented in Supplementary Table S2-S3.

3. Results and discussion

3.1. Preparation and characterization of FRCS NPs

Based on the inherent characteristics of the erythrocyte membrane, a surface-modified erythrocyte membrane carrier system was constructed to utilize the targeted delivery of PTX for tumor chemotherapy. The synthetic procedure for biomimetic FRCS NPs consisted of three steps: 1) Hydrophilic CMC and hydrophobic SA were self-assembled into CMCS NPs (inner core). 2) Membrane-derived vesicles were prepared from natural erythrocytes according to previously reported methods [47–49]. FA was then modified to membrane-derived vesicles to prepare FA-RBCM (envelope). 3) FA-RBCM was used to encapsulate CMCS NPs, thus forming a new type of biomimetic FRCS NPs. This biomimetic NDDS could proactively translocate to tumor tissues and sense pH variations in the microenvironment. After degradation, PTX was released by the biomimetic FRCS NPs, which strengthened the antitumor effects and alleviated the potential side effects of PTX (Fig. 1). The core of the CMCS NPs is a two-block amphoteric polymer composed of hydrophilic CMC and hydrophobic SA prepared by the self-assembly method (Fig. 1a). The successful synthesis of CMCS was confirmed by the characteristic signals in the proton nuclear magnetic resonance (¹H NMR) spectrum (Fig. S1a). More importantly, compared to the core that are directly grafting PEG onto PTX [50], we used CMC and SA to form a two-block amphoteric polymer, which could avoid PTX's premature release and decrease its non-specific accumulation in the peripheral organs. Given that the folic acid/folate receptor axis serves as a molecular target for epithelial malignancy treatment [51,52], RBCMs were obtained from the mouse blood by the hypotonic method, followed by a functionalized modification with DSPE-PEG-FA on their surfaces to enhance the targeting ability (Fig. 1b and c). Although DSPE functions as a lipid tether, it may decrease the concealment of NPs, leading to its sequestration by RES and MPS [34,44]. To avoid this, we utilized the PEGylation modification, which is regarded as a superior method of preparing "stealth" NPs, thus reducing the RES- and MPS-mediated NP capture and prolonging the NP circulating time [53–55]. Therefore, we embed PEG into DSPE-FA to form a triblock DSPE-PEG-FA polymer to improve the "stealth" of RBCMs. Furthermore, surface modification of RBCMs was verified by ¹H NMR (Fig. S1b). Finally, FA-grafted RBCMs were mixed with CMCS NPs in a unified system for further ultrasonic crushing and coaxial extrusion to obtain biomimetic FRCS NPs.

Next, we verified the physical and chemical characteristics of biomimetic FRCS NPs. As shown in Fig. 2a and Fig. S2a, TEM analysis revealed that CMCS and RBCM NPs were spherical and uniform. Interestingly, the FRCS NPs showed distinct core-shell spherical structures when compared to naked CMCS NPs. Morphologically, FRCS NPs were characterized by CMCS NPs, which were surrounded by a gray and white ring composed of RBCM. The thickness of the homogeneous outer membrane shell was approximately 10 nm, suggesting successful coating of the erythrocyte membrane. Additionally, Malvern Zetasizer analysis showed that CMCS NPs had an average size of 163.8 ± 2.22 nm and a negative Zeta potential of -17.6 ± 0.4 mV, guaranteeing passive

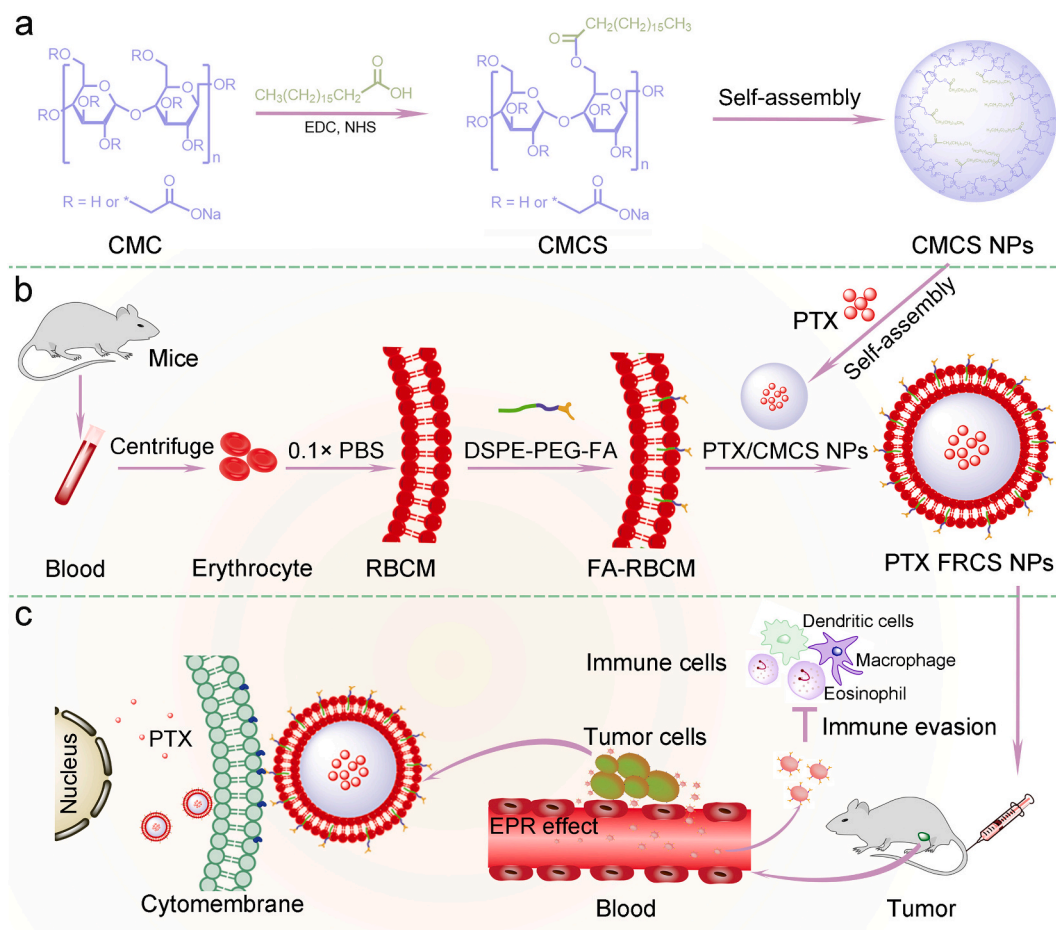


Fig. 1. (a) and (b) Schematic illustration of the preparation of CMCS NPs and PTX FRCS NPs. (c) Biomimetic FRCS NPs are further used for enhanced in vivo tumor chemotherapy therapy.

targeting to tumor sites. After the fusion of CMCS NPs and RBC vesicles, the final average size and the Zeta potential of FRCS NPs increased to 226.9 ± 2.75 nm and -14.5 ± 0.3 mV, respectively (Fig. 2b, Supplementary Table S4). Notably the negative charges of the FRCS NPs prevented their unexpected aggregation because of charge repulsion.

Furthermore, natural polysaccharide CMCS NPs with endogenous molecules on their surfaces can prolong blood circulation, immune escape, and homotypic targeting ability in the body. To confirm the successful translocation of RBCMs onto the proposed CMCS NPs, we systematically tested the protein profile of the NP surface via protein sodium dodecyl sulfate-polyacrylamide gel electrophoresis (SDS-PAGE). As shown in Fig. 2c, unmodified and FA-modified RBCs showed similar physicochemical properties, suggesting that surface modification of DSPE-PEG-FA modestly affected the properties of RBCMs. More importantly, when compared to CMCS NPs, FRCS NPs possessed a protein profile similar to that of erythrocyte membrane derivation, indicating that the proteins of RBCMs were successfully transferred onto CMCS NPs. In addition, to examine the integrity of the coating process, we examined the protein expression of CD47, a representative RBC transmembrane protein, on the FRCS NPs. As shown in Fig. 2d, western blot analysis revealed that distinct CD47 bands (50 kDa) were present in both the source erythrocyte membrane derivation (Line I) and RBCM/FRCS NPs (Lines II and IV). To determine whether the extracted membrane protein orientation was corrected, we used specific antibodies against the N-terminal (extracellular) domain of CD47 and found that the CD47 N-terminal is abundantly expressed on the surface of FRCS NPs (Fig. S2b).

Lastly, given that the extracellular domain of CD47 is responsible for

the immune-evasive RBC properties [42], we incubated the RAW264.7 macrophages with FRCS NPs to check the particle internalization. FACS analysis revealed that the RBCM coating rendered the particles less prone to macrophage uptake (Fig. 2e and f). The reduced susceptibility indicated that the immune evasive function was indeed translocated from RBCMs to FRCS NPs. In contrast, functional blockage of the CD47 N-terminal restored the particle internalization ability of RAW264.7 macrophages, further confirming that the orientation of the extracted membrane protein was corrected. Theoretically, owing to the abundant sialylated moieties, the extracellular side of RBCMs exerts a strong negative charge [56]. Considering the electrostatic effects, the negatively charged core of the FRCS NPs favors interaction with the less negatively charged intracellular side of the RBCMs, thus producing a potential orientation bias [42]. This orientation bias may increase the possibility of a right-side-out membrane orientation on the FRCS NPs.

3.2. Drug loading and release

The encapsulation efficiency (EE) of FRCS NPs for PTX was examined by changing the PTX dose. As shown in Fig. S2c, the EE of FRCS NPs depended on the PTX dose and tended to be consistent with 15 mg PTX. When the ratio of FRCS NP/PTX reached 5:6, the system was regarded satisfactory. The loading efficiency and EE% of PTX were 11.5% and 96.8%, respectively. Additionally, to address the biocompatibility of the CMCS NPs and FRCS NPs, a serum stability analysis was performed, and we found that an expansion occurred in the particle size of CMCS NPs over 24 h (Fig. 3a), indicating that the RBCM coating increased the stability of core CMCS NPs. To further detect the pH sensitivity of FRCS

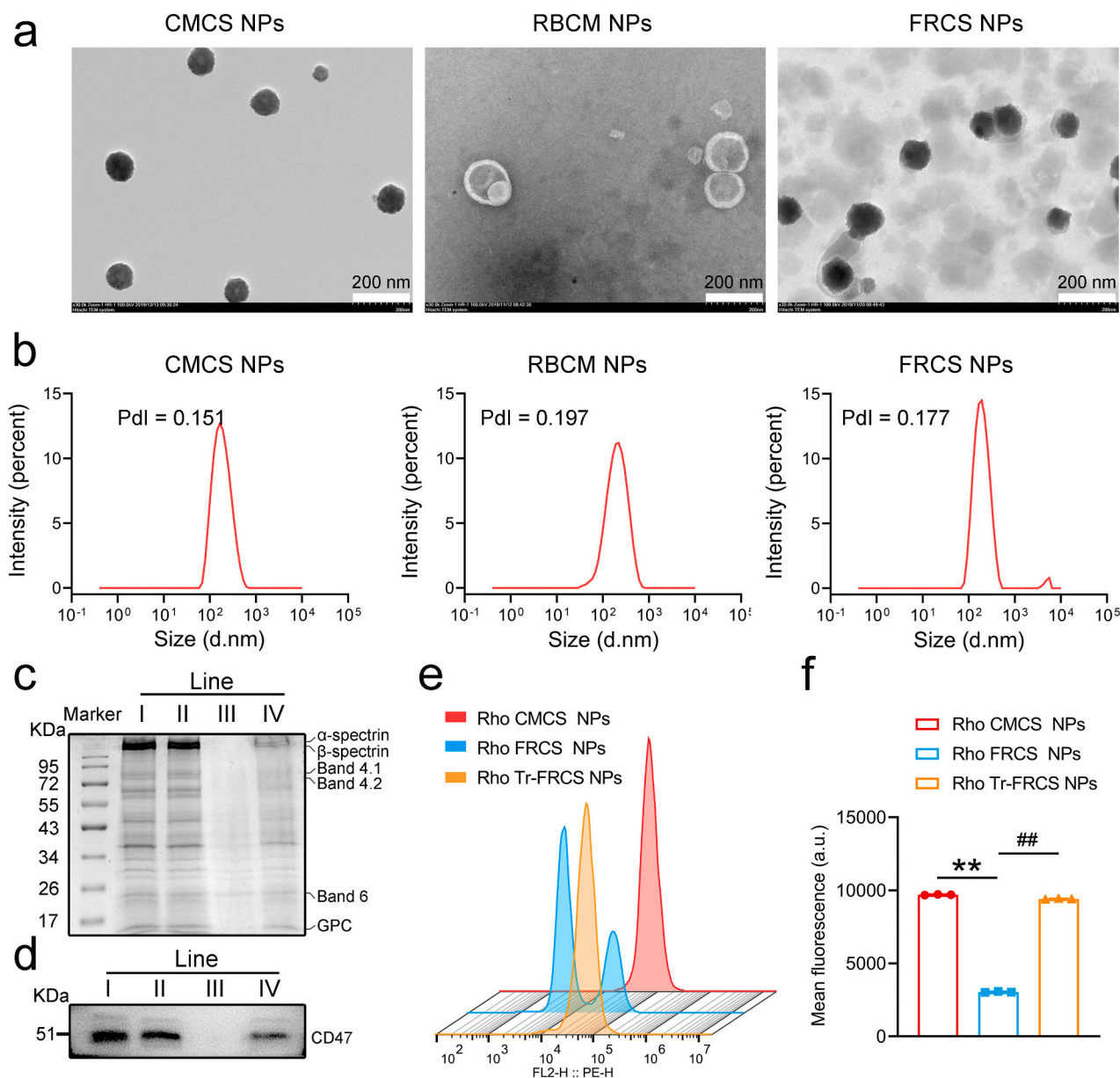


Fig. 2. Characterization of NPs. (a) Representative TEM images of CMCS NPs, RBCM NPs and FRCS NPs. (b) The size of NPs measured at pH = 7.4 by Malvern Laser Particle Analyzer. (c) SDS-PAGE analysis of RBC (I), RBCM NPs (II), CMCS NPs (III), and FRCS NPs (IV). (d) Western blot analysis of CD47. (e) Flow cytometry analysis of particle internalization by RAW264.7 macrophages. (f) Mean fluorescence intensity reflecting the overall particle uptake by macrophage. Data were presented as mean \pm SD ($n = 5$). One-way ANOVA with Tukey's post-hoc test. $**p < 0.01$ vs. Rho CMCS NPs group, $##p < 0.01$ vs. Rho FRCS NPs group.

NPs, the release kinetics of PTX were measured in a milieu simulating the acidic tumor microenvironment. Intriguingly, when the pH value decreased from 7.4 (physiological condition) to 5.5 (tumor acidic condition), the FRCS NPs showed a significant increase in the accumulative release plateau of PTX, indicating that the FRCS NP system was an acidic pH-sensitive NDDS (Fig. 3b). Hence, when FRCS NPs enter the tumor core, they can be ruptured by the acidic tumor microenvironment and release functional PTX to kill tumor cells. In addition, PTX was more sensitively released from non-coated CMCS NPs in either the tumor acidic or physiological microenvironment when compared to that from FRCS NPs (Fig. 3b). These results indicate that our RBC membrane protected PTX and prevented its non-specific release in the circulating system, especially under physiological conditions.

3.3. Cellular distribution and uptake of FRCS NPs

The cellular distribution and uptake of NPs determine their ability for intracellular drug delivery [57]. As shown in Fig. 3c, the internalization of Cy5-labeled FRCS NPs in cancer cells was clearly observed. Pretreatment of cells with caveolae-dependent cell uptake inhibitors, such as filipin, significantly disrupted the cellular uptake of Cy5-labeled FRCS NPs, whereas chlorpromazine (CPA, a clathrin-mediated endocytosis inhibitor) and EIPA (a macropinocytosis inhibitor) showed modest effects. Collectively, these data suggest that caveolae-dependent cellular internalization plays an essential role in the cellular internalization of FRCS NPs.

3.4. Tumor targeting efficiency of the FRCS NPs in vivo

On the other hand, in vivo biodistribution assay was performed to

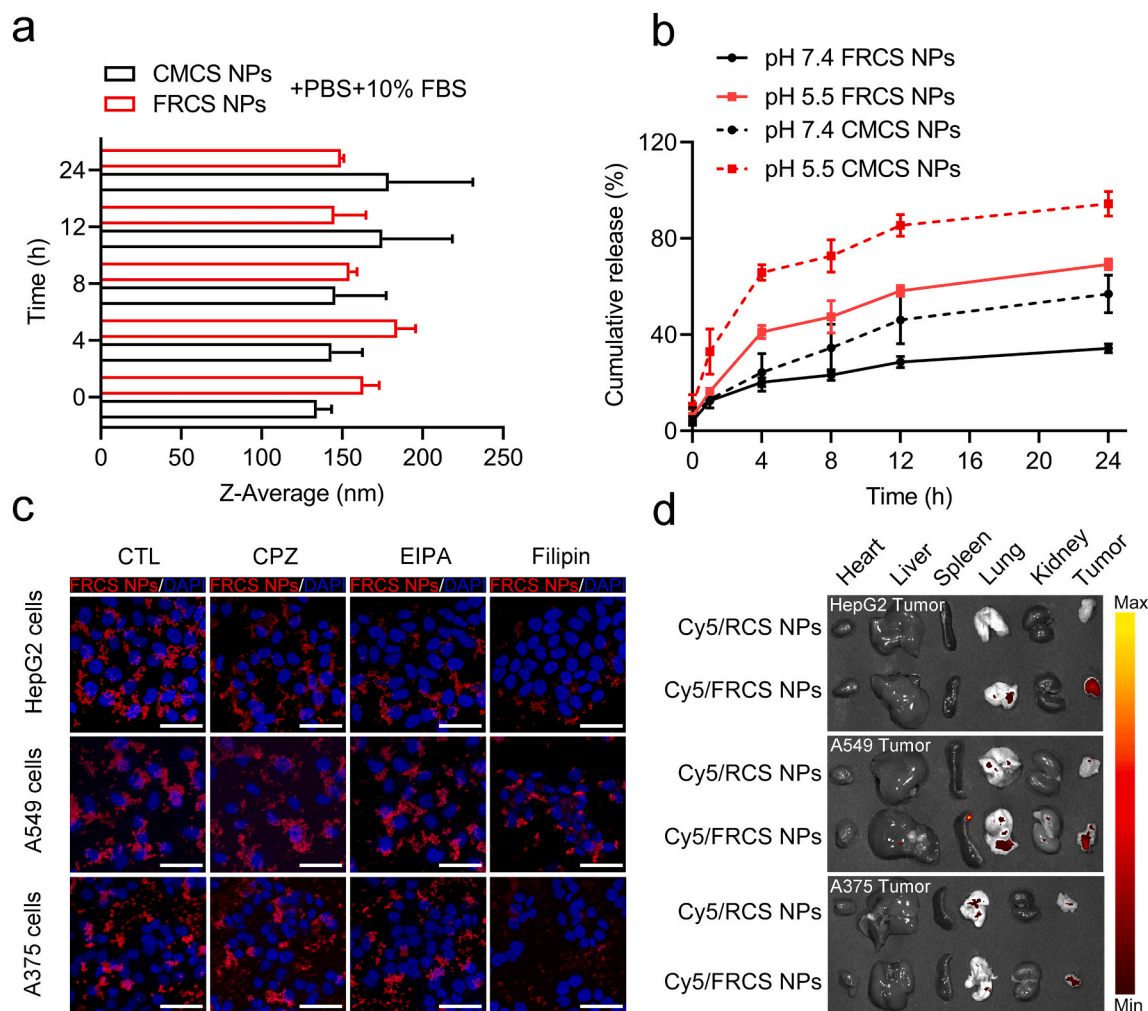


Fig. 3. (a) The stability of FRCS NPs. (b) The cumulative release profile of PTX from FRCS NPs. (c) Representative confocal laser scanning microscopy images of cancer cells (HepG2 cells, A549 cells and A375 cells) treated with either Cy5-labeled FRCS NPs alone or in combination with indicated inhibitors. (d) Fluorescence imaging analysis of the biodistribution of the FCA NPs in vivo.

evaluate the potential application of the developed FRCS NPs. Next, we conducted a biodistribution study of typical epithelial malignancies, including liver cancer, lung cancer, and melanoma. As shown in Fig. 3d, FRCS NPs remarkably accumulated within the tumor xenografts for at least 24 h. In addition, the fluorescence signals of FRCS NPs were observed in the lungs, further substantiating the “stealth” properties the RBCM endows in the circulating system [58]. Note that these fluorescence signals nearly undetectable in other organs, such as the liver, suggesting that PEGylation modified-RBCM contributed to the FRCS NPs’ escape from the hepatic RES system-mediated capture, which prolonging the NP circulating time.

Notably, the accumulation of FA-enabled FRCS NPs was 2-fold higher than that of RCS NPs in all the diseased tumor tissues (Fig. S2d). Taken together, biomimetic FRCS NPs are biocompatible and potentially immuno-escaped; hence, they possess improved sustained-release and tumor-targeting abilities.

3.5. Biosafety analysis of FRCS NPs

To evaluate the safety of FRCS NPs in vivo, we intravenously injected FRCS NPs into C57BL6/J mice for 21 d. As shown in Fig. S3a and b, both body weight and food intake of mice were affected by FRCS NPs when compared to the PBS-treated control group. Because drug-induced liver injury accounts for more than 50% of acute liver failure prevalence in the clinic, the evaluation of liver function is of great importance for drug

safety [59]. Therefore, the serum levels of liver injury-related parameters, including ALT and AST, were detected, and no significant differences were found between the two groups, indicating that FRCS NPs were safe for liver function in mice (Fig. S3c). Simultaneously, H&E staining showed that the liver tissue cells of the mice had a complete structure and clear morphology (Fig. S3d). In addition, in vitro analysis confirmed that FRCS NPs did not alter the viability of primary mouse hepatocytes (Fig. S3e). Taken together, these results suggest that FRCS NPs exhibit satisfactory biosafety and are suitable for PTX delivery.

3.6. Evaluation of the antitumor activity in vitro and in vivo

Given the active tumor-targeting ability of FRCS NPs, we next explored their potential application in delivering chemotherapeutic PTX into epithelial tumors. We selected typical epithelial tumor cell lines, including HepG2 hepatoma, A549 lung cancer, and A375 melanoma cells, to study the in vitro antitumor efficacy of PTX FRCS NPs. As shown in Fig. 4a, CCK-8 analyses revealed that either PTX or PTX FRCS NPs administration dose-dependently decreased the cell viabilities of all tested cells when compared the CTL treatment. Importantly, as evidenced by the IC_{50} calculation, PTX FRCS NP administration exhibited more drastic inhibitory effects than PTX alone. Additionally, FRCS NPs did not affect the viability of all tested cancer cells, indicating that the synergistic inhibitory effect of PTX FRCS NPs was not caused by the potential toxicity of FRCS NPs on these cells (Fig. S4). Next, we

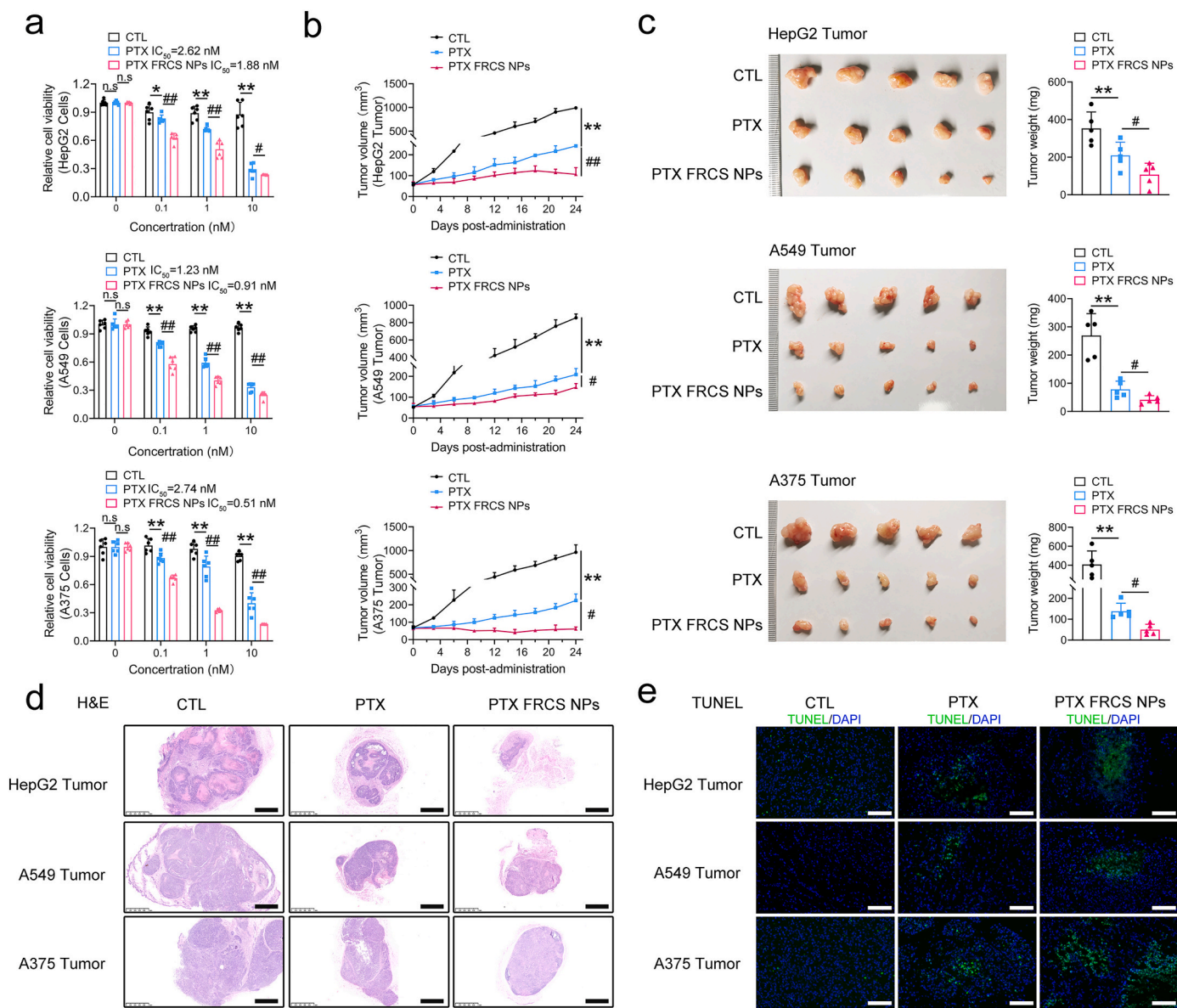


Fig. 4. The evaluation of the antitumor activity in vitro and in vivo. (a) Cell viability of cancer cells (HepG2 cells, A549 cells and A375 cells) treated with various drug groups. Data were presented as mean ± SD (n = 5). One-way ANOVA with Tukey’s post-hoc test. **p* < 0.05, ***p* < 0.01 vs. CTL group, #*p* < 0.05, ##*p* < 0.01 vs. free PTX group. (b) Tumor growth curve during chemotherapy. (c) Left: Images of tumor tissues dissected after treatment. Right: Tumor weights. (d) H&E staining of tumor tissues. Scale bar = 1 mm. (e) TUNEL staining of tumor tissues. Scale bar = 50 μm. Data were presented as mean ± SD (n = 5). One-way ANOVA with Tukey’s post-hoc test (b and c). **p* < 0.05, ***p* < 0.01 vs. CTL group, #*p* < 0.05, ##*p* < 0.01 vs. free PTX group.

evaluated the antitumor efficiency of PTX FRCS NPs in vivo using a subcutaneous xenograft tumor-bearing mouse model. As shown in Fig. 4b and c, the administration of either free PTX or PTX FRCS NPs significantly decreased the growth of xenograft tumors. Similar to the in vitro results, PTX FRCS NPs exhibited statistical repressive properties in all xenograft tumors. We found that the tumor weights of both A549 and A375 tumor tissues free of PTX and PTX in NPs were indeed different. The inhibitory ratios of tumor weights were 48.7%, 47%, and 30.7% for PTX FRCS NP-treated xenograft tumors of HepG2, A549, and A375 cells, respectively, when compared to those in the groups treated with free PTX (Fig. 4c). In addition, H&E staining analyses revealed that administration of PTX FRCS NPs decreased tumor cell density and blurred tumor cell borders when compared to the free PTX-treated groups (Fig. 4d). TUNEL analyses further confirmed that FRCS NPs could strengthen the antitumor properties of PTX (Fig. 4e). Note that although our morphological data did not significantly differ between the two groups, the characteristics of the tumor tissues were altered in PTX FRCS

NP-treated mice. Thus, we believe that FRCS NPs increased the anti-tumor effects of PTX on these xenograft tumors.

Considering that biosafety is an important factor in determining the potential for translational medicine, we evaluated this in xenograft tumor-bearing mice treated with either PTX alone or PTX FRCS NPs. We found that the body weights of the FRCS NP-treated groups were modestly affected compared to the CTL-treated group (Fig. S5a–c). Meanwhile, the serum levels of transaminases were not altered by drug treatments (Fig. S5d–i). Additionally, no remarkable histological or pathological abnormalities were observed in the various organs, including the heart, liver, spleen, and lungs (Fig. S6). However, PTX has been documented to possess multiple side effects when accumulated in the kidney [60]. To address this issue, we first examined the serum indicators of renal function, including creatinine (CRE) and blood urea nitrogen (BUN). We found that the serum CRE and BUN levels were significantly increased in the mice treated with PTX alone compared with those in the control group, whereas they were decreased in the

biomimetic FRCS NP-treated group (Fig. 5a). H&E staining and TUNEL analyses revealed that FRCS NPs alleviated PTX-induced renal toxicity, as evidenced by the alleviation of pathological characteristics, including tubular dilatation, cast formation, brush border loss (Fig. S7), and fewer TUNEL-positive renal cells in the kidneys of mice treated with PTX FRCS NPs than in the kidneys of mice treated with PTX alone (Fig. 5b). At the molecular level, PTX increased the mRNA expression levels of renal injury biomarkers such as *Ngal* and *Kim-1* (Fig. 5c). By contrast, PTX FRCS NPs significantly abrogated this induction. The above results indicated that PTX FRCS NPs significantly inhibited tumor growth while reducing PTX toxicity, especially in the kidney.

Finally, PTX is known to induce the secretion of inflammatory cytokines, which cause systemic inflammation and an immune response

[61,62]. Therefore, we quantified the levels of secreted inflammatory cytokines, including interleukin-6 (IL-6), IL-12, interferon- γ (IFN- γ), and tumor necrosis factor- α (TNF- α), in the serum of all experimental mouse models. As shown in Fig. 5d, administration of PTX alone significantly increased inflammatory cytokine secretion, whereas the biomimetic FRCS NPs retarded it. This beneficial amelioration may be explained by the fact that the biomimetic FRCS NPs functionally deliver PTX into tumors, thereby reducing the unexpected circulating PTX, which decreases nonspecific biodistribution in vivo.

4. Conclusions

In summary, an erythrocyte membrane-camouflaged polysaccharide

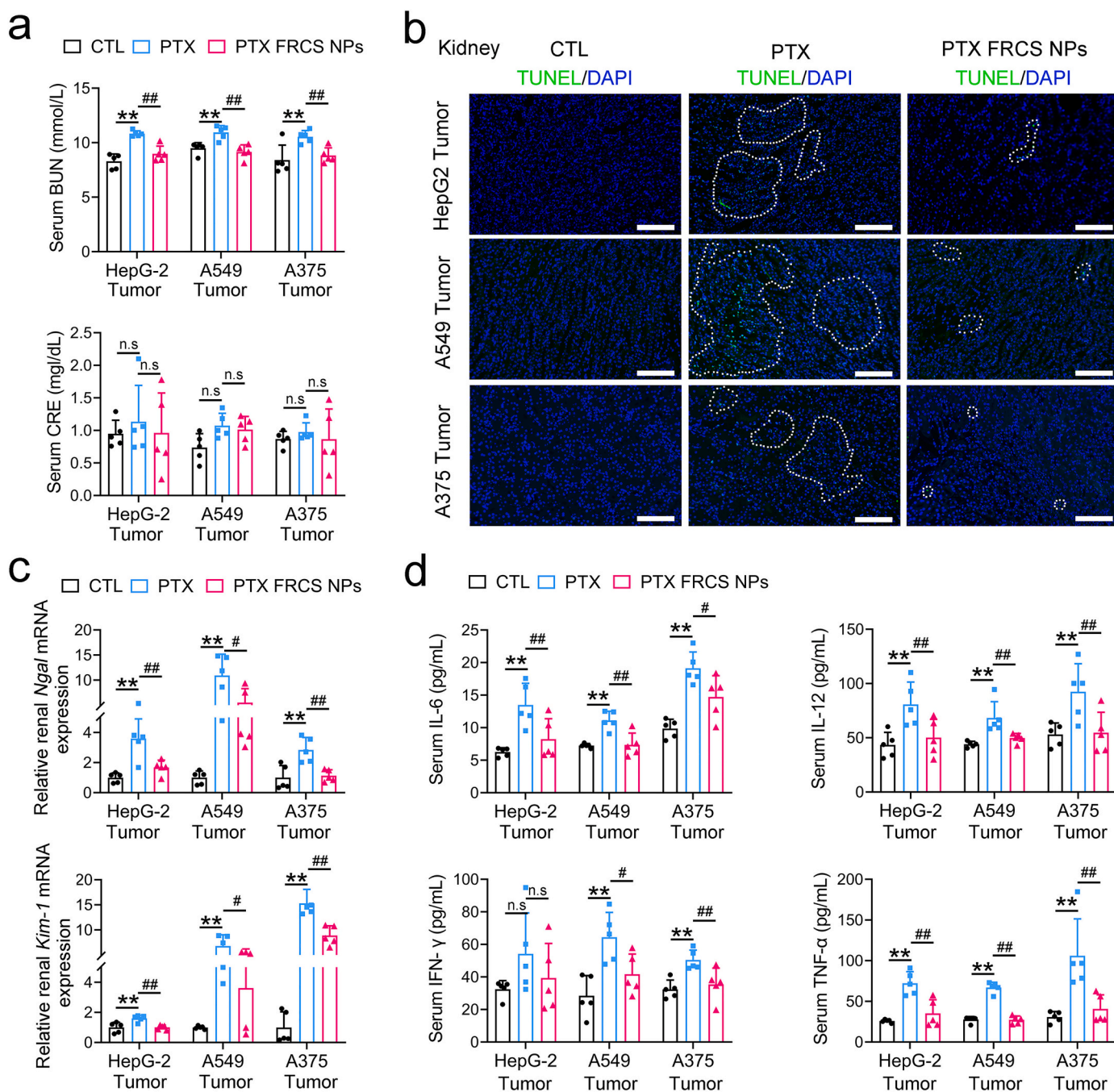


Fig. 5. Renal safety assessment and immune response analyses of the nanocarrier. (a) Serum levels of BUN and CRE. (b) TUNEL staining of kidney. (c) RT-qPCR analyses of *Ngal* and *Kim-1* mRNA expression in the mouse kidney. (d) Serum levels of IL-6, IL-12, INF- γ and TNF- α . Data were presented as mean \pm SD (n = 5). One-way ANOVA with Tukey's post-hoc test (a, c, and d). * p < 0.05, ** p < 0.01 vs. CTL group, # p < 0.05, ## p < 0.01 vs. free PTX group.

NP was used in epithelial cancer therapy. Using the membrane cloaking approach, the merits of an erythrocyte membrane were incorporated into polysaccharide NPs, which improved biocompatibility and prolonged circulation time. Our FRCS NP system functionally delivered PTX to the tumor sites to achieve precise treatment of epithelial malignant tumors while alleviating the side effects of PTX, particularly in the kidney. Undoubtedly, considering the abundant availability of RBCs in the host blood, the basal materials for the shell of this NDDS are easily obtained and avoid the synthesis of a “protein crown” induced by the core PTX CMCS NPs. Collectively, the proposed FRCS NP system is a promising drug delivery vector for decreasing the immune responses and undesirable side effects of chemotherapeutic drugs for further clinical applications, including, but not limited to, epithelial cancer treatment.

Credit author statement

Mingming Song, Xiao Li and Siyu Chen conceived the project. Mingming Song, Shuqi Dong, Xiaofei An, and Wenxiang Zhang performed the experiments. Mingming Song, Chang Liu and Siyu Chen wrote the manuscript, prepared the figures and was responsible for data compilation and integration. Ning Shen, Yanbo Li, and Caixia Guo contributed to reanalyze the raw data using multiple comparison methods. All authors contributed significant feedback and additions. All authors have given approval to the final version of the manuscript.

Declaration of Competing Interest

None.

Acknowledgments

This work was financially supported by grants from the National Natural Science Foundation of China (31800992 to S. C., 92057112 and 31771298 to C. L., 81800512 to W. Z., 81774248 to X. A.), the Project of State Key Laboratory of Natural Medicines, China Pharmaceutical University (SKLNMZZ202005 to C. L.), and the Fundamental Research Funds for the Central Universities (2632022ZD08 to W. Z.), the Priority Academic Program Development of Jiangsu Higher Education Institutions (PAPD, to S. C., C. L. and W. Z.).

Appendix A. Supplementary data

Supplementary data to this article can be found online at <https://doi.org/10.1016/j.jconrel.2022.03.060>.

References

- [1] D. Ribatti, R. Tamma, T. Anness, Epithelial-mesenchymal transition in cancer: a historical overview, *Transl. Oncol.* 13 (2020), 100773.
- [2] T. Jiang, G. Xu, G. Chen, Y. Zheng, B. He, Z. Gu, Progress in transdermal drug delivery systems for cancer therapy, *Nano Res.* 13 (2020) 1810–1824.
- [3] G. Lin, R.A. Revia, M. Zhang, Inorganic nanomaterial-mediated gene therapy in combination with other antitumor treatment modalities, *Adv. Funct. Mater.* 31 (2021) 2007096.
- [4] T. Anani, S. Rahmati, A.E.D. Nayer Sultana, MRI-traceable theranostic nanoparticles for targeted cancer treatment, *Theranostics* 11 (2021) 579.
- [5] T. do Nascimento, A.R. Todeschini, R. Santos-Oliveira, D.B.M. de Souza, S. Mariana, V.T. de Souza, E. Ricci-Júnior, Trends in nanomedicines for cancer treatment, *Curr. Pharm. Des.* 26 (2020) 3579–3600.
- [6] S.K. Rehman, J. Haynes, E. Collignon, K.R. Brown, Y. Wang, A.M.L. Nixon, J. P. Bruce, J.A. Wintersinger, A. Singh Mer, E.B.L. Lo, C. Leung, E. Lima-Fernandes, N.M. Pedley, F. Soares, S. McGibbon, H.H. He, A. Pollet, T.J. Pugh, B. Haibe-Kains, Q. Morris, M. Ramalho-Santos, S. Goyal, J. Moffat, C.A. O'Brien, Colorectal cancer cells enter a diapause-like DTP state to survive chemotherapy, *Cell* 184 (2021) 226–242 e221.
- [7] C. Bailly, X. Thuru, B. Quesnel, Combined cytotoxic chemotherapy and immunotherapy of cancer: modern times, *NAR Cancer* 2 (2020) zcaa002.
- [8] C. Gebhardt, S.C.S. Simon, R. Weber, M. Gries, D.H. Mun, R. Reinhard, T. Holland-Letz, V. Umansky, J. Utikal, Potential therapeutic effect of low-dose paclitaxel in melanoma patients resistant to immune checkpoint blockade: a pilot study, *Cell. Immunol.* 360 (2021), 104274.
- [9] S. Huang, L. Deng, H. Zhang, L. Wang, Y. Zhang, Q. Lin, T. Gong, X. Sun, Z. Zhang, L. Zhang, Co-delivery of TRAIL and paclitaxel by fibronectin-targeting liposomal nanodisk for effective lung melanoma metastasis treatment, *Nano Res.* (2021) 1–10.
- [10] S. Zhang, Z. Yang, F. Qi, Aldehyde dehydrogenase-positive melanoma stem cells in tumorigenesis, drug resistance and anti-neoplastic immunotherapy, *Mol. Biol. Rep.* 47 (2020) 1435–1443.
- [11] J. Wang, W. Qiao, H. Zhao, J. Cheng, Y. Han, X. Yang, A highly atom-economical bioactive nanocarrier for synergistically enhanced antitumor with reduced liver injury, *New J. Chem.* 44 (2020) 16741–16751.
- [12] Z.L. Lin, J. Ding, G.P. Sun, D. Li, S.S. He, X.F. Liang, X.R. Huang, J. Xie, Application of paclitaxel-loaded EGFR peptide-conjugated magnetic polymeric liposomes for liver cancer therapy, *Curr. Med. Sci.* 40 (2020) 145–154.
- [13] S. Huang, L. Deng, H. Zhang, L. Wang, Y. Zhang, Q. Lin, T. Gong, X. Sun, Z. Zhang, L. Zhang, Co-delivery of TRAIL and paclitaxel by fibronectin-targeting liposomal nanodisk for effective lung melanoma metastasis treatment, *Nano Res.* 15 (1) (2021) 728–737.
- [14] S. Huang, Y. Zhang, L. Wang, W. Liu, L. Xiao, Q. Lin, T. Gong, X. Sun, Q. He, Z. Zhang, L. Zhang, Improved melanoma suppression with target-delivered TRAIL and paclitaxel by a multifunctional nanocarrier, *J. Control. Release* 325 (2020) 10–24.
- [15] D. Kashyap, H.S. Tuli, M.B. Yerer, A. Sharma, K. Sak, S. Srivastava, A. Pandey, V. K. Garg, G. Sethi, A. Bishayee, Natural product-based nanoformulations for cancer therapy: opportunities and challenges, *Semin. Cancer Biol.* 69 (2021) 5–23.
- [16] V.J. Yao, S. D'Angelo, K.S. Butler, C. Theron, T.L. Smith, S. Marchio, J.G. Gelovani, R.L. Sidman, A.S. Dobroff, C.J. Brinker, A.R.M. Bradbury, W. Arap, R. Pasqualini, Ligand-targeted theranostic nanomedicines against cancer, *J. Control. Release* 240 (2016) 267–286.
- [17] B.L. Banik, P. Fattahi, J.L. Brown, Polymeric nanoparticles: the future of nanomedicine, *Wiley Interdiscip. Rev. Nanomed. Nanobiotechnol.* 8 (2016) 271–299.
- [18] S. Gao, T. Li, Y. Guo, C. Sun, B. Xianyu, H. Xu, Selenium-containing nanoparticles combine the NK cells mediated immunotherapy with radiotherapy and chemotherapy, *Adv. Mater.* 32 (2020), e1907568.
- [19] H. Kang, S. Rho, W.R. Stiles, S. Hu, Y. Baek, D.W. Hwang, S. Kashiwagi, M.S. Kim, H.S. Choi, Size-dependent EPR effect of polymeric nanoparticles on tumor targeting, *Adv. Healthc. Mater.* 9 (2020), e1901223.
- [20] C. Xu, F. Haque, D.L. Jasinski, D.W. Binzel, D. Shu, P. Guo, Favorable biodistribution, specific targeting and conditional endosomal escape of RNA nanoparticles in cancer therapy, *Cancer Lett.* 414 (2018) 57–70.
- [21] M. Song, W. Xia, Z. Tao, B. Zhu, W. Zhang, C. Liu, S. Chen, Self-assembled polymeric nanocarrier-mediated co-delivery of metformin and doxorubicin for melanoma therapy, *Drug Deliv.* 28 (2021) 594–606.
- [22] A. Angelopoulou, A. Kolokithas-Ntoukas, C. Fytas, K. Avgoustakis, Folic acid-functionalized, condensed magnetic nanoparticles for targeted delivery of doxorubicin to tumor cancer cells overexpressing the folate receptor, *ACS Omega* 4 (2019) 22214–22227.
- [23] B. Pelaz, C. Alexiou, R.A. Alvarez-Puebla, F. Alves, A.M. Andrews, S. Ashraf, L. P. Balogh, L. Ballerini, A. Bestetti, C. Brendel, S. Bosi, M. Carril, W.C. Chan, C. Chen, X. Chen, X. Chen, Z. Cheng, D. Cui, J. Du, C. Dullin, A. Escudero, N. Feliu, M. Gao, M. George, Y. Gogotsi, A. Grunweller, Z. Gu, N.J. Halas, N. Hampp, R. K. Hartmann, M.C. Hersam, P. Hunziker, J. Jian, X. Jiang, P. Jungebluth, P. Kadhiresan, K. Kataoka, A. Khademhosseini, J. Kopecek, N.A. Kotov, H.F. Krug, D.S. Lee, C.M. Lehr, K.W. Leong, X.J. Liang, M. Ling Lim, L.M. Liz-Marzan, X. Ma, P. Macchiariini, H. Meng, H. Mohwald, P. Mulvaney, A.E. Nel, S. Nie, P. Nordlander, T. Okano, J. Oliveira, T.H. Park, R.M. Penner, M. Prato, V. Punties, V.M. Rotello, A. Samarakoon, R.E. Schaak, Y. Shen, S. Sjoqvist, A.G. Skirtach, M. G. Soliman, M.M. Stevens, H.W. Sung, B.Z. Tang, R. Tietze, B.N. Udagama, J. S. VanEpps, T. Weil, P.S. Weiss, I. Willner, Y. Wu, L. Yang, Z. Yue, Q. Zhang, Q. Zhang, X.E. Zhang, Y. Zhao, X. Zhou, W.J. Parak, Diverse applications of nanomedicine, *ACS Nano* 11 (2017) 2313–2381.
- [24] F. Madani, S.S. Esnaashari, B. Mujokoro, F. Dorkoosh, M. Khosravani, M. Adabi, Investigation of effective parameters on size of paclitaxel loaded PLGA nanoparticles, *Adv. Pharm. Bull.* 8 (2018) 77–84.
- [25] H. Xin, X. Sha, X. Jiang, L. Chen, K. Law, J. Gu, Y. Chen, X. Wang, X. Fang, The brain targeting mechanism of Angiopep-conjugated poly(ethylene glycol)-co-poly(epsilon-caprolactone) nanoparticles, *Biomaterials* 33 (2012) 1673–1681.
- [26] H. Sun, J. Su, Q. Meng, Q. Yin, L. Chen, W. Gu, P. Zhang, Z. Zhang, H. Yu, S. Wang, Y. Li, Cancer-cell-biomimetic nanoparticles for targeted therapy of homotypic tumors, *Adv. Mater.* 28 (2016) 9581–9588.
- [27] M.M. Abeer, P. Rewatkar, Z. Qu, M. Talekar, F. Kleitz, R. Schmid, M. Linden, T. Kumeria, A. Popat, Silica nanoparticles: a promising platform for enhanced oral delivery of macromolecules, *J. Control. Release* 326 (2020) 544–555.
- [28] M.J. Mitchell, M.M. Billingsley, R.M. Haley, M.E. Wechsler, N.A. Peppas, R. Langer, Engineering precision nanoparticles for drug delivery, *Nat. Rev. Drug Discov.* 20 (2021) 101–124.
- [29] T. Miao, J. Wang, Y. Zeng, G. Liu, X. Chen, Polysaccharide-based controlled release systems for therapeutics delivery and tissue engineering: from bench to bedside, *Adv. Sci.* 5 (2018) 1700513.
- [30] M. Fathi, E.D. Abdolahinia, J. Barar, Y. Omid, Smart stimuli-responsive biopolymeric nanomedicines for targeted therapy of solid tumors, *Nanomedicine-Uk* 15 (2020) 2171–2200.

- [31] Y. Sheng, J. Gao, Z.-Z. Yin, J. Kang, Y. Kong, Dual-drug delivery system based on the hydrogels of alginate and sodium carboxymethyl cellulose for colorectal cancer treatment, *Carbohydr. Polym.* 118325 (2021).
- [32] M. Xie, J. Li, T. Deng, N. Yang, M. Yang, Modification of magnetic molybdenum disulfide by chitosan/carboxymethylcellulose with enhanced dispersibility for targeted photothermal-/chemotherapy of cancer, *J. Mater. Chem. B* 9 (2021) 1833–1845.
- [33] F. Ofridam, M. Tarhini, N. Lebaz, É. Gagnière, D. Mangin, A. Elaissari, pH-sensitive polymers: classification and some fine potential applications, *Polym. Adv. Technol.* 32 (2021) 1455–1484.
- [34] B. Ouyang, W. Poon, Y.N. Zhang, Z.P. Lin, B.R. Kingston, A.J. Tavares, Y. Zhang, J. Chen, M.S. Valic, A.M. Syed, P. MacMillan, J. Couture-Senechal, G. Zheng, W.C. W. Chan, The dose threshold for nanoparticle tumour delivery, *Nat. Mater.* 19 (2020) 1362–1371.
- [35] R. Cai, C. Chen, The crown and the scepter: roles of the protein corona in nanomedicine, *Adv. Mater.* 31 (2019) 1805740.
- [36] C.M. Hu, L. Zhang, S. Aryal, C. Cheung, R.H. Fang, L. Zhang, Erythrocyte membrane-camouflaged polymeric nanoparticles as a biomimetic delivery platform, *Proc. Natl. Acad. Sci. U. S. A.* 108 (2011) 10980–10985.
- [37] V.R. Muzykantov, Drug delivery by red blood cells: vascular carriers designed by mother nature, *Exp. Opin. Drug Deliv.* 7 (2010) 403–427.
- [38] S. Aryal, C. Hu, R. Fang, D. Dehaini, C. Carpenter, D. Zhang, L. Zhang, Erythrocyte membrane-cloaked polymeric nanoparticles for controlled drug loading and release, *Nanomedicine-Uk* 8 (2013) 1271–1280.
- [39] Q. Xia, Y. Zhang, Z. Li, X. Hou, N. Feng, Red blood cell membrane-camouflaged nanoparticles: a novel drug delivery system for antitumor application, *Acta Pharm. Sin. B* 9 (2019) 675–689.
- [40] G.M.N. Neubi, Y. Opoku-Damoah, X. Gu, Y. Han, J. Zhou, Y. Ding, Bio-inspired drug delivery systems: an emerging platform for targeted cancer therapy, *Biomater. Sci.* 6 (2018) 958–973.
- [41] F.G. Baudou, L. Fusco, E. Giorgi, E. Diaz, S. Muncioy, M.F. Desimone, L. Leiva, M. C. De Marzi, Physicochemical and biological characterization of nanovenoms, a new tool formed by silica nanoparticles and *Crotalus durissus terrificus* venom, *Colloids Surf. B: Biointerfaces* 193 (2020), 111128.
- [42] C.M. Hu, R.H. Fang, B.T. Luk, K.N. Chen, C. Carpenter, W. Gao, K. Zhang, L. Zhang, 'Marker-of-self' functionalization of nanoscale particles through a top-down cellular membrane coating approach, *Nanoscale* 5 (2013) 2664–2668.
- [43] G. Yu, T.R. Cook, Y. Li, X. Yan, D. Wu, L. Shao, J. Shen, G. Tang, F. Huang, X. Chen, P.J. Stang, Tetraphenylethene-based highly emissive metallacage as a component of theranostic supramolecular nanoparticles, *Proc. Natl. Acad. Sci. U. S. A.* 113 (2016) 13720–13725.
- [44] Y. Liu, Y. Hu, L. Huang, Influence of polyethylene glycol density and surface lipid on pharmacokinetics and biodistribution of lipid-calcium-phosphate nanoparticles, *Biomaterials* 35 (2014) 3027–3034.
- [45] J.-M. Liu, D.-D. Zhang, G.-Z. Fang, S. Wang, Erythrocyte membrane bioinspired near-infrared persistent luminescence nanocarriers for in vivo long-circulating bioimaging and drug delivery, *Biomaterials* 165 (2018) 39–47.
- [46] M. Kang, J. Hong, M. Jung, S.P. Kwon, S.Y. Song, H.Y. Kim, J.R. Lee, S. Kang, J. Han, J.H. Koo, J.H. Ryu, S. Lim, H.S. Sohn, J.M. Choi, J. Doh, B.S. Kim, T-cell-mimicking nanoparticles for cancer immunotherapy, *Adv. Mater.* 32 (2020), e2003368.
- [47] H. Cabral, K. Kataoka, Erythrocyte depletion lifts nanoparticle half-lives, *Nat. Biomed. Eng.* 4 (2020) 670–671.
- [48] M.P. Nikitin, I.V. Zelepukin, V.O. Shipunova, I.L. Sokolov, S.M. Deyev, P.I. Nikitin, Enhancement of the blood-circulation time and performance of nanomedicines via the forced clearance of erythrocytes, *Nat. Biomed. Eng.* 4 (2020) 717–731.
- [49] M. He, P. Yu, Y. Hu, J. Zhang, M. He, C. Nie, X. Chu, Erythrocyte-membrane-enveloped biomimetic metal-organic framework nanoparticles enable intravenous glucose-responsive insulin delivery, *ACS Appl. Mater. Interfaces* 13 (2021) 19648–19659.
- [50] Z. Zhai, P. Xu, J. Yao, R. Li, L. Gong, Y. Yin, Z. Lin, Erythrocyte-mimicking paclitaxel nanoparticles for improving biodistributions of hydrophobic drugs to enhance antitumor efficacy, *Drug Deliv.* 27 (2020) 387–399.
- [51] R. Geetha Bai, K. Muthoosamy, R. Tuvikene, H. Nay Ming, S. Manickam, Highly sensitive electrochemical biosensor using folic acid-modified reduced graphene oxide for the detection of cancer biomarker, *Nanomaterials* 11 (2021) 1272.
- [52] N. Tang, H. Li, L. Zhang, X. Zhang, Y. Chen, H. Shou, S. Feng, X. Chen, Y. Luo, R. Tang, A macromolecular drug for cancer therapy via extracellular calcification, *Angew. Chem. Int. Ed.* 60 (2021) 6509–6517.
- [53] X.-J. Du, J.-L. Wang, W.-W. Liu, J.-X. Yang, C.-Y. Sun, R. Sun, H.-J. Li, S. Shen, Y.-L. Luo, X.-D. Ye, Regulating the surface poly (ethylene glycol) density of polymeric nanoparticles and evaluating its role in drug delivery in vivo, *Biomaterials* 69 (2015) 1–11.
- [54] Y. Sheng, C. Liu, Y. Yuan, X. Tao, F. Yang, X. Shan, H. Zhou, F. Xu, Long-circulating polymeric nanoparticles bearing a combinatorial coating of PEG and water-soluble chitosan, *Biomaterials* 30 (2009) 2340–2348.
- [55] T. Liu, H. Choi, R. Zhou, I.W. Chen, RES blockade: a strategy for boosting efficiency of nanoparticle drug, *Nano Today* 10 (2015) 11–21.
- [56] K.M. Jan, S. Chien, Role of surface electric charge in red blood cell interactions, *J. Gen. Physiol.* 61 (1973) 638–654.
- [57] L. Yu, M. Xu, W. Xu, W. Xiao, X.-H. Jiang, L. Wang, H. Gao, Enhanced cancer-targeted drug delivery using precoated nanoparticles, *Nano Lett.* 20 (2020) 8903–8911.
- [58] Y. Fu, W. Liu, L.-Y. Wang, B.-Y. Zhu, M.-K. Qu, L.-Q. Yang, X. Sun, T. Gong, Z.-R. Zhang, Q. Lin, L. Zhang, Erythrocyte-membrane-camouflaged nanopatform for intravenous glucose-responsive insulin delivery, *Adv. Funct. Mater.* 28 (2018).
- [59] M. Garcia-Cortes, M. Robles-Diaz, C. Stephens, A. Ortega-Alonso, M.I. Lucena, R. J. Andrade, Drug induced liver injury: an update, *Arch. Toxicol.* 1-27 (2020).
- [60] J.S. Baek, J.H. Kim, J.S. Park, C.W. Cho, Modification of paclitaxel-loaded solid lipid nanoparticles with 2-hydroxypropyl-beta-cyclodextrin enhances absorption and reduces nephrotoxicity associated with intravenous injection, *Int. J. Nanomedicine* 10 (2015) 5397–5405.
- [61] M. Luo, L. Dong, J. Li, Y. Wang, B. Shang, Protective effects of pentoxifylline on acute liver injury induced by thioacetamide in rats, *Int. J. Clin. Exp. Pathol.* 8 (2015) 8990.
- [62] P. Wang, H. Wang, Q. Huang, C. Peng, L. Yao, H. Chen, Z. Qiu, Y. Wu, L. Wang, W. Chen, Exosomes from M1-polarized macrophages enhance paclitaxel antitumor activity by activating macrophages-mediated inflammation, *Theranostics* 9 (2019) 1714.